

PADRINO, J.C., SRINIL, N., KURUSHINA, V., SWAILES, D., PAIN, C.C. and MATAR, O.K. 2021. A one-dimensional mechanistic model for tracking unsteady slug flow. In *Proceedings of the 2021 ASME international mechanical engineering congress and exposition (IMECE2021)*, 1-5 November 2021, [virtual event]. New York: ASME [online], volume 10: fluids engineering, article number V010T10A004. Available from: <https://doi.org/10.1115/IMECE2021-70735>

A one-dimensional mechanistic model for tracking unsteady slug flow.

PADRINO, J.C., SRINIL, N., KURUSHINA, V., SWAILES, D., PAIN, C.C. and MATAR, O.K.

2021

©ASME. All rights reserved. This is the accepted manuscript version of the above paper. The published version of record is available for purchase from the ASME website:
<https://doi.org/10.1115/IMECE2021-70735>

IMECE2021-70735

A ONE-DIMENSIONAL MECHANISTIC MODEL FOR TRACKING UNSTEADY SLUG FLOW

Juan C. Padrino^a, Narakorn Srinil^a, Victoria Kurushina^a, David Swailes^b,
Christopher C. Pain^c, Omar K. Matar^d

^aMarine, Offshore and Subsea Technology Group, School of Engineering, Newcastle University

^bSchool of Mathematics, Statistics and Physics, Newcastle University
Newcastle upon Tyne, United Kingdom

^cDepartment of Earth Science and Engineering, Imperial College London

^dDepartment of Chemical Engineering, Imperial College London
London, United Kingdom

ABSTRACT

A novel one-dimensional slug tracking mechanistic model for unsteady, upward gas-liquid slug flow in inclined pipes is presented. The model stems from the first principles of mass and momentum conservation applied to a slug unit cell consisting of a slug body of liquid and a region of stratified flow containing an elongated bubble and a liquid film. The slug body front and rear are treated as surfaces of discontinuity where mass and momentum balances or “jump laws” are prescribed. The former is commonly applied in mechanistic models for slug flow, whereas the latter is typically overlooked, thereby leading to the assumption of a continuous pressure profile at these points or to the adoption of a pressure drop due to the fluid acceleration on a heuristic basis. Our analysis shows that this pressure change arises formally from the momentum jump law at the slug body front. The flow is assumed to be isothermal, the gas is compressible, the pressure drop in the elongated bubble region is accounted for, the film thickness is considered uniform, and weight effects in the pressure from the interface level are included. Besides specifying momentum jump laws at both borders of the slug body, another novel feature of the present model is that we avoid adopting the quasi-steady approximation for the elongated bubble-liquid film region, and thus the unsteady terms in the mass and momentum

balances are kept. The present model requires empirical correlations for the slug body length and the elongated bubble nose velocity. The non-linear equations are discretized and solved simultaneously for all the slug unit cells filling the pipe. Time-space variation of the slug body and film lengths, liquid holdup and void fraction, and pressures, among other quantities, can be predicted, and model performance is evaluated by comparing with data in the literature.

INTRODUCTION

Depending on the geometric features of the pipeline conveying a mixture of liquid (oil and water) and gas, the fluids properties, and their flow rates, the slug flow pattern — characterized by an alternate distribution of gas- and liquid-dominant phases — may prevail. In an oil-and-gas production system, the reliability of separation and pumping equipment downstream of the pipe is known to be strongly affected by the size and dynamics of slug bodies. Because the presence of slug flow entails the possibility of flow assurance issues, including the costs of operational interruption, the development and improvement of tools for the accurate modeling of slug flow continues to be of interest to the industry. In particular, models capable of predicting the transient

behavior of the slug units as they travel along the pipe may prove useful especially in conditions where the conduit’s vibrational motions are significant, as in the presence of resonance, or if the maximum slug length and not only the average is sought.

Mechanistic models have the advantage of enforcing mass, momentum, and energy conservation laws in one dimension. They also include some empirically-based relationships for closure. Among the various mechanistic models for steady slug flow proposed in the literature, we list here the works due to [1–4]. Comprehensive reviews have been presented by [5, 6].

To model variations of slug length and frequency as the slug unit travels along a pipe, as well as slug formation, dissipation, and bubble overtaking, unsteady slug flow approaches are needed. Models for unsteady slug flow can be classified in three categories, namely, “slug capturing” models, which are based upon the two-fluid model for segregated flows and are effective at describing slug formation, but are commonly very computationally demanding [7, 8]; “slug tracking” models, which draw significantly from the mechanistic models developed for steady slug flow and can be considered the extension of this approach to the unsteady situation (see literature survey in [9]), and the “hybrid models”, which combine both approaches (see the review in [10]).

Here, we focus on the slug tracking. The works that use this approach that are more relevant to us are those by Nydal and Banerjee [11], Al-safran *et al.* [12], Ujang *et al.* [13], Rosa *et al.* [9], and the very recent one by Grigoletto *et al.* [14]. By comparing against experimental data, the performance of the various models is evaluated and regarded as satisfactory, in general. Nonetheless, in all these models, with the exception of [11], the so-called quasi-steady or quasi-equilibrium approximation is adopted. This approximation consists on significantly simplifying the system of equations by dropping some of the unsteady terms in the mass and momentum balances as well as momentum fluxes in the latter. In [12, 13] the steady momentum equations of [2, 15] with constant film thickness are used for the liquid film and elongated bubble regions of a slug flow unit and also the steady version of the momentum balance is applied to the slug body or liquid slug. In [9, 14], the rate of change of momentum in the slug body — but not in the film or elongated bubble — as well as momentum fluxes are considered. Specifically, in [14], a term accounting for momentum fluxes is included as an additional pressure difference modeling the head loss caused by liquid recirculation in the elongated bubble wake.

The work that has the closest similarities with the present effort is that by [11]. They consider unsteady mass balances for the slug body, the liquid film — of uniform film thickness — and elongated bubble regions, whilst applying unsteady momentum balances to the first two regions. On the other hand, their approach differs with ours in that they assume a uniform pressure in the gas bubble region, enabling them to discard the gas momentum equation, and do not describe spatial variations in the

liquid film velocity.

In this paper, we formulate a one-dimensional mechanistic model for slug tracking in horizontal or inclined pipes (upward flow) applied to unsteady gas-liquid flow. It is based on integral mass and momentum balances where the unsteady terms and momentum fluxes are kept in all regions of the flow and in both mass and momentum balances. Specifically, the main novelties in the model are the following. First, no quasi-equilibrium assumption is made in the description of the stratified region of the slug flow. Even though the liquid film thickness in the stratified region of the slug unit is assumed uniform, preserving unsteadiness in the mass conservation equations for the liquid film and elongated bubble regions leads to axially varying *in-situ* velocities in the fluids. We are not aware that this result has been presented in the literature on mechanistic modeling of slug flow. Second, the transitions between the slug body and stratified regions are modeled as surfaces of discontinuity where not only mass but also momentum balances are imposed; this results in pressure jumps at these locations. Third, the numerical solution is fully implicit.

The article is organized as follows. In the next section, the model formulation is described. This is followed by the numerical treatment and the model applications with preliminary results and discussion. We then conclude with some final remarks.

MODEL FORMULATION

We model the slug flow in a pipeline as a sequence of slug unit cells. A sketch of a typical slug unit cell is shown in Fig. 1. The unit cell of gas-liquid slug flow denoted with index j is bounded between positions x^{j+1} and x^j ; the elongated bubble-liquid film combined region is limited by positions x^{j+1} and y^j , and the film thickness is assumed to be uniform; the liquid slug, which in this work — and as in the case of [9, 11] — is considered without small bubbles, falls between positions y^j and x^j . These positions are measured with respect to the pipe inlet. The liquid slug length, a function of time, is denoted by l_s and is given by $x^j - y^j$. The film length l_f is given by $y^j - x^{j+1}$ and may also change with time. The flow along the pipeline is assumed isothermal. The gas density is assumed to be a function of gas pressure and computed with the ideal gas law. In the derivations that follow, we consider the liquid and gas densities, ρ_l^j and ρ_g^j , respectively, to be uniform within slug unit cell j and they can be a function of time. They may change from one unit cell to the other due to spatial pressure changes. The liquid and gas viscosities are assumed constant and denoted by μ_l and μ_g , respectively. The length of the entire unit cell is $l_u = l_f + l_s$. The unit cell is considered to be contained in a straight pipe element whose axis is inclined at angle θ with respect to the horizontal direction. The pipe has a circular cross section with area A and diameter D assumed invariant along the pipeline. The acceleration of gravity points downward and is perpendicular to the horizontal direction. Here, we confine ourselves to the case of a straight pipe, so that

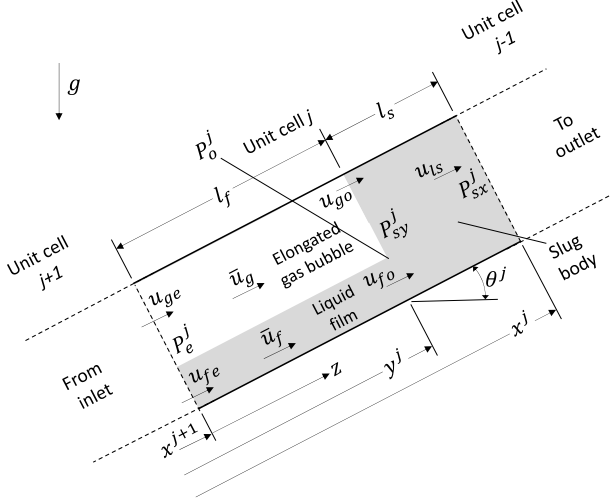


FIGURE 1. SKETCH OF A TYPICAL SLUG FLOW UNIT CELL. TWO-PHASE GAS-LIQUID SLUG FLOW IS MODELED AS A SEQUENCE OF UNIT CELLS.

θ is uniform.

The position of a unit cell at any time t is tracked by the following relations

$$\dot{y}^j = \frac{dy^j}{dt} = u_t^j, \quad (1)$$

where u_t^j is the translational velocity of the elongated bubble nose in unit cell j and

$$\dot{x}^j = \frac{dx^j}{dt}. \quad (2)$$

The integral mass and momentum balances that follow are written using the formulae for a control volume and for a surface of discontinuity exhibiting arbitrary motion presented in [16] and extended here for two-phase gas-liquid flow.

Mass balances

Mass balance for the slug body belonging to slug unit cell j with no gas in it, in a pipe of constant cross-sectional area, yields a liquid velocity, u_{ls}^j , that does not change from the slug front to its tail, and that is thus a function of time only. Integral mass balances over expanding or contracting control volumes encompassing the liquid film and the elongated bubble regions lead to the following one-dimensional conservation statements. For the

liquid film, we can write

$$\frac{d}{dt} (\rho_l^j \bar{\alpha}_f^j l_f^j A) = \rho_l^j \bar{\alpha}_f^j A (u_{fe}^j - \dot{x}^{j+1}) - \rho_l^j \bar{\alpha}_f^j A (u_{fo}^j - u_t^j). \quad (3)$$

Here, $\bar{\alpha}_f^j$ is the holdup of the liquid film, which has constant thickness; u_{fo}^j and u_{fe}^j denote the axial film velocities at positions y^j and x^{j+1} , respectively. Substitution of $dl_f^j/dt = u_t^j - \dot{x}^{j+1}$ results in

$$\frac{d}{dt} (\rho_l^j \bar{\alpha}_f^j) = \frac{\rho_l^j \bar{\alpha}_f^j}{l_f^j} (u_{fe}^j - u_{fo}^j). \quad (4)$$

Consider a control volume of arbitrary length z within the liquid film of slug unit j (Fig. 1), having the same thickness as the film, with $0 \leq z \leq l_f^j$ and such that, if $z = 0$, this plane moves as x^{j+1} and, if $z = l_f^j$, this plane moves as y^j . For this control volume, we can write the mass balance:

$$z \frac{d}{dt} (\rho_l^j \bar{\alpha}_f^j) = \rho_l^j \bar{\alpha}_f^j (u_{fe}^j - u_f^j), \quad (5)$$

where u_f^j is the film velocity at z . Eliminating the time derivatives between (4) and (5) yields

$$u_f^j = (1 - z/l_f^j)u_{fe}^j + (z/l_f^j)u_{fo}^j, \quad (6)$$

which upon integration over the entire film length leads to the average velocity in the film

$$\bar{u}_f^j = (u_{fo}^j + u_{fe}^j) / 2. \quad (7)$$

For the gas in the elongated bubble,

$$\frac{d}{dt} (\rho_g^j \bar{\alpha}_g^j) = \frac{\rho_g^j \bar{\alpha}_g^j}{l_f^j} (u_{ge}^j - u_{go}^j), \quad (8)$$

where $\bar{\alpha}_g^j$, u_{go}^j , and u_{ge}^j are analogous to $\bar{\alpha}_f^j$, u_{fo}^j , and u_{fe}^j used in the liquid film — $\bar{\alpha}_g^j$ denotes the void fraction. Proceeding in an similar manner as in the case of the liquid film results in

$$u_g^j = (1 - z/l_f^j)u_{ge}^j + (z/l_f^j)u_{go}^j, \quad (9)$$

and

$$\bar{u}_g^j = (u_{go}^j + u_{ge}^j)/2. \quad (10)$$

Eqs. (6), (7), (9), and (10) seem to be new. Both \bar{u}_f^j and \bar{u}_g^j will appear in the momentum equations, so the relations for these averages, which do not seem as an obvious result to us, will prove useful. When the time derivatives in (4) and (8) vanish, we recover the classical result for a film of uniform thickness, namely, $u_{fo}^j = u_{fe}^j = \bar{u}_f^j$ and the velocity is uniform in the film. Analogous conclusions can be drawn for the gas bubble.

At position x^j , consider a surface of discontinuity. We can write the liquid and gas mass balances, respectively,

$$\rho_l^{j-1} \bar{\alpha}_f^{j-1} (u_{fe}^{j-1} - \dot{x}^j) = \rho_l^j (u_{ls}^j - \dot{x}^j), \quad (11)$$

$$u_{ge}^{j-1} = \dot{x}^j. \quad (12)$$

whilst, at position y^j ,

$$\rho_l^j (u_{ls}^j - u_t^j) = \rho_l^j \bar{\alpha}_f^j (u_{fo}^j - u_t^j), \quad (13)$$

$$u_t^j = u_{ge}^j, \quad (14)$$

Note that (12) and (14) hold because there is no gas in the slug bodies.

Finally, the geometric constraint is

$$\bar{\alpha}_f^j + \bar{\alpha}_g^j = 1. \quad (15)$$

Momentum balances

One-dimensional expressions for momentum conservation can be obtained from integral linear momentum balances over expanding or contracting control volumes including the slug body, the liquid film or the elongated bubble regions. For the liquid slug body, we can write

$$\frac{d}{dt} (\rho_l^j u_{ls}^j) = \frac{(P_{sy}^j - P_{sx}^j)}{l_s^j} - \tau_s^j \frac{\pi D}{A} - \rho_l^j g \sin \theta, \quad (16)$$

where P_{sx}^j and P_{sy}^j are the pressure at x^j and y^j on the side of the slug body, respectively. Specifically, this pressure corresponds to the pipe axis. Also, τ_s^j is the shear stress at the wall, and g is the acceleration of gravity. In writing (16), we started with the rate of change of momentum in the slug body, $d(\rho_l^j u_{ls}^j l_s^j A)/dt = l_s^j Ad(\rho_l^j u_{ls}^j)/dt + \rho_l^j u_{ls}^j Adl_s^j/dt$. After using

$dl_s^j/dt = \dot{x}^j - u_t^j$, the last term cancels the momentum fluxes in the momentum balance. Then, by dividing the resulting expression with $l_s^j A$, we obtain (16).

For the liquid film, momentum conservation can be written as

$$\begin{aligned} \frac{d}{dt} (\rho_l^j \bar{\alpha}_f^j \bar{u}_f^j) &= -\frac{\rho_l^j \bar{\alpha}_f^j}{l_f^j} (u_t^j - \dot{x}^{j+1}) \bar{u}_f^j \\ &+ \frac{\rho_l^j \bar{\alpha}_f^j}{l_f^j} (u_{fe}^j - \dot{x}^{j+1}) u_{fe}^j - \frac{\rho_l^j \bar{\alpha}_f^j}{l_f^j} (u_{fo}^j - u_t^j) u_{fo}^j \\ &+ \frac{\bar{\alpha}_f^j (P_e^j - P_o^j)}{l_f^j} - \bar{\tau}_f^j \frac{S_f^j}{A} + \bar{\tau}_i^j \frac{S_i^j}{A} - \rho_f^j \bar{\alpha}_f^j g \sin \theta. \end{aligned} \quad (17)$$

In the starting point leading to equation (17), we write the momentum conservation with the rate of change of momentum in the control volume as $d(\rho_l^j \bar{\alpha}_f^j \bar{u}_f^j l_f^j A)/dt$ in the left-hand side, which is expanded as $l_f^j Ad(\rho_l^j \bar{\alpha}_f^j \bar{u}_f^j)/dt + \rho_l^j \bar{\alpha}_f^j \bar{u}_f^j Adl_f^j/dt$. The latter is moved to the right-hand side; dividing by $l_f^j A$ yields (17).

Similarly, for the elongated gas bubble, the momentum conservation can be written as

$$\begin{aligned} \frac{d}{dt} (\rho_g^j \bar{\alpha}_g^j \bar{u}_g^j) &= -\frac{\rho_g^j \bar{\alpha}_g^j}{l_f^j} (u_t^j - \dot{x}^{j+1}) \bar{u}_g^j \\ &+ \frac{\bar{\alpha}_g^j (P_e^j - P_o^j)}{l_f^j} - \bar{\tau}_g^j \frac{S_g^j}{A} - \bar{\tau}_i^j \frac{S_i^j}{A} - \rho_g^j \bar{\alpha}_g^j g \sin \theta. \end{aligned} \quad (18)$$

In these expressions, P_o^j and P_e^j denote the pressure on faces y^j and x^{j+1} on the side of the elongated bubble-film combined region, respectively. Specifically, this pressure corresponds to the elongated bubble-film interface at the associated axial location. Moreover, $\bar{\tau}$ is the average shear stress, S is the perimeter, and their subscripts f, g, i refer to the liquid film, elongated bubble, and bubble-film interface, respectively. The average velocities \bar{u}_f^j and \bar{u}_g^j are given by (7) and (10), respectively.

In the same manner as we did for mass conservation in (11)-(14), we can write momentum balances at x^j and y^j — treated as surfaces of discontinuity (e.g., see section 5.18 in [16]). At position x^j ,

$$\begin{aligned} P_e^{j-1} + \rho_l^{j-1} \bar{\alpha}_f^{j-1} (u_{fe}^{j-1} - \dot{x}^j) u_{fe}^{j-1} + \rho_g^{j-1} \bar{\alpha}_g^{j-1} (u_{ge}^{j-1} - \dot{x}^j) u_{ge}^{j-1} \\ + (\rho_l^{j-1} \bar{\alpha}_f^{j-1} \xi_f^{j-1} - \rho_g^{j-1} \bar{\alpha}_g^{j-1} \xi_g^{j-1}) g \cos \theta \\ = P_{sx}^j + \rho_l^j (u_{ls}^j - \dot{x}^j) u_{ls}^j. \end{aligned} \quad (19)$$

At position y^j ,

$$P_{sy}^j + \rho_l^j (u_{ls}^j - u_t^j) u_{ls}^j = P_o^j + \rho_l^j \bar{\alpha}_f^j (u_{fo}^j - u_t^j) u_{fo}^j + \rho_g^j \bar{\alpha}_g^j (u_{go}^j - u_t^j) u_{go}^j + (\rho_l^j \bar{\alpha}_f^j \xi_f^j - \rho_g^j \bar{\alpha}_g^j \xi_g^j) g \cos \theta, \quad (20)$$

where

$$\bar{\alpha}_f^j A \xi_f^j = \int_{A_f} (h_f - \zeta) dA, \quad \bar{\alpha}_g^j A \xi_g^j = \int_{A_g} (\zeta - h_f) dA. \quad (21)$$

Here, ζ is the coordinate of a point at a given cross section measured from the lowermost point in the cross section and h_f is the film thickness. These integrals bring into the model the hydrostatic effect of the film level accounting for gradual pressure variations in the direction orthogonal to the pipe's axis. Eqs. (19) and (20) can be simplified by making use of (11)-(14). The pressure difference arising in (19) bear some resemblance to the acceleration pressure gradient usually introduced in the literature in a somewhat heuristic manner (e.g., see [1]). Here, it appears as a "jump law" from a formal momentum balance across a surface of discontinuity at x^j .

The average shear stresses at the wall and at the interface needed in (17) and (18) are computed by integration of the local shear stresses, which in turn are determined from the local fluid velocities given in (6) and (9) using suitable closures (see next sub-section). The wall shear stress in the slug body is evaluated with the same closure relationship in terms of velocity u_{ls}^j and the liquid properties.

The gas density at the elongated bubble of slug unit cell j is computed with the average pressure $(P_o^j + P_e^j)/2$.

Closure and geometric relationships

To provide closure to the system of equations formed by the conservation equations, we invoke some relationships from the literature obtained by fitting experimental data. In addition, we use a few geometric relationships describing the stratified elongated bubble-film region. The expressions we include are well known; hence we do not reproduce them here.

For the shear stresses, we use the relationships in [2] which are written in terms of the Fanning friction factor. These factors are determined by means of the Blasius formula for smooth pipes (see [17]) for the stresses at the wall. For the interfacial friction factor, we use the value of 0.014 [2, 18]. For the bubble nose translational velocity, we apply the correlation used by [12] based on a result of [19], which includes a wake function describing the effect of accelerating the nose of a bubble. Finally, for the length of the liquid slug body, we use the correlation given in [4].

The geometric relationships describing the elongated bubble-film cross section can be readily derived by considering a

circular cross section containing a gas-liquid stratified configuration with a flat interface and the liquid at the bottom. We can then establish relations between the angle subtended by the gas-liquid interface and the gas and film wetted perimeters, S_g and S_f , interface length S_i , film thickness, h_f , and liquid holdup and void fraction, $\bar{\alpha}_f$ and $\bar{\alpha}_g$. They can be found, for instance, in [6,9,13]. The integrals in (21) are evaluated based on this configuration.

NUMERICAL ASPECTS

For a slug unit cell, the proposed model contains 20 unknowns, namely, $\{P_{sx}, \dot{x}, x, u_{ls}, P_{sy}, u_t, y, P_o, u_{fo}, u_{go}, \bar{u}_f, \bar{u}_g, \rho_g, P_e, u_{fe}, u_{ge}, \bar{\alpha}_f, \bar{\alpha}_g, l_f, l_s\}$. The model comprises 20 equations per slug unit cell; these are expressions (1), (2), (4), (7), (8), (10), (11), (12), (13), (14), (15), (16), (17), (18), (19), (20), the equation for the bubble nose translational velocity, the equation of state for the gas density, and relations $l_s^j = x^j - y^j$ and $l_f^j = y^j - x^{j+1}$.

The ordinary differential equations in time are discretized with a first order implicit backward Euler scheme. For example, for the mass conservation equation in the elongated gas bubble, Eq. (8), we obtain

$$\left(\rho_g^{j(n+1)} \alpha_g^{j(n+1)} - \rho_g^{j(n)} \alpha_g^{j(n)} \right) - \Delta t \frac{\rho_g^{j(n+1)} \alpha_g^{j(n+1)}}{l_f^{j(n+1)}} \left(u_{ge}^{j(n+1)} - u_{go}^{j(n+1)} \right) = 0, \quad (22)$$

where Δt is the time step and n and $n+1$ are the time levels. The values at time level $n+1$ are unknown whilst those at level n are known. The variables in the expressions in the model that are not differential equations are considered at time level $n+1$. Accordingly, unit cells' external and internal borders are advanced with $x^{j(n+1)} = x^{j(n)} + \Delta t \dot{x}^{j(n+1)}$ and $y^{j(n+1)} = y^{j(n)} + \Delta t u_t^{j(n+1)}$. Lengths are then determined with $l_s^{j(n+1)} = x^{j(n+1)} - y^{j(n+1)}$ and $l_f^{j(n+1)} = y^{j(n+1)} - x^{j+1(n+1)}$. Regarding the average shear stresses, they are obtained by numerical integration using sixteen-point standard Gauss-Legendre quadrature (e.g., see [20,21]).

A fully-implicit solution of the resulting non-linear system of equations is sought using the non-linear solver available in Matlab[®]. This package applies an algorithm based on the Newton method. We provide a vector of residuals to the solver, where each residual consists of the left-hand side of an algebraic equation from the model when this equation is written in such a way that the right-hand side is equal to zero, as in Eq. (22). The residuals are nondimensionalized using as scales the liquid density, the gas density at the outlet pressure, the mixture velocity at the inlet, $j_l + j_g$, as the velocity scale, the product of the liquid density times the square of the inlet mixture velocity as the pressure

scale, and $10D$ as the length scale. The vector of results from the previous time step is given to the non-linear solver as the initial guessed values. These are passed to the solver nondimensionalized using the aforementioned scales. They are converted back to dimensional form in order to compute the residuals.

The Jacobian is computed numerically using finite differences with a tolerance of $\approx 10^{-6}$. Because this is a one-dimensional model, we arrange the vector of residuals and the vector of guessed values such that the Jacobian matrix is block-diagonal. We take advantage of this fact by providing to the solver a sparsity pattern consisting of an array of ones, indicating the elements in the Jacobian that are nonzero. This significantly reduces the computational time (e.g., see [22]).

As boundary conditions, at the pipe exit we impose a constant pressure, whilst at the inlet we use the inlet superficial velocities j_l and j_g and the fluids properties to generate a slug unit cell using our model without the unsteady terms. This is supplemented, for closure, with the expression relating the liquid superficial velocity with the amount of liquid in a unit cell passing through a fix pipe cross section (Eq. 5 in [2]). Once the tail of the elongated bubble reaches the pipe inlet, a new slug unit cell is created as just described. Once the entering slug unit has been created, it evolves based on the model for unsteady flow presented here (unsteady approach of first slug unit). An alternative, following [14], is to consider this slug unit as steady until its bubble nose touches the inlet. This can be achieved here by dropping the terms in the equations modeling the rate of change of mass and momentum in the various control volumes. When we apply this, we do it only for the first slug unit (steady approach). Equations (11)-(12) are enforced at the tail of the entering elongated bubble-film region (position $x^{(N_u+1)}$), setting $u_{ls}^{(N_u+1)} = j_l + j_g$, where N_u refers to the slug unit entering the pipe.

For the slug unit cell exiting the pipe, once its slug body front reaches this position, its length will start to gradually decrease. When the nose of the following elongated bubble touches the exit, the magnitudes of its translational velocity u_t and pressure P_o are set to remain fixed and the elongated bubble-film region will continue to move as if the pipe length were extended. Note that [9] “froze” the attributes of the leading slug unit cell once its slug body front reaches the pipe exit. On the other hand, [14] instantaneously removed the elongated bubble and liquid film following a slug body that has just left the pipe.

Initially, the pipe is filled with liquid flowing steadily with velocity j_l . The liquid-only section of the pipe preceding the first slug unit is modeled by splitting it into control volumes or cells, typically of length $8D$. We assume that the borders of these cells, with no loss of generality, move with the translational velocity of the first elongated bubble — including the first slug body front. The border of the liquid-only cell coinciding with the exit has $\dot{x} = 0$. Then, this cell’s length decreases; when it reaches a threshold ($2D$), this cell merges with the following one. The liquid-only

Run	j_l (m s ⁻¹)	j_g (m s ⁻¹)	D (mm)
1	0.20	0.15	38
2	0.73	0.15	38
3	0.73	0.44	38
4	0.73	0.73	38
5	0.73	0.44	67
6	0.73	1.17	67

TABLE 1. EXPERIMENTAL RUNS FOR HORIZONTAL SLUG FLOW OF GAS AND LIQUID IN A PIPE. EXTRACTED FROM [23].

cells are modeled with a momentum equation similar to that of the slug body, Eq. (16). The liquid in these cells move with the velocity of the liquid in the first slug body, $u_{ls}^{(1)}$. The pressure is continuous across the cell’s borders shared by two liquid-only cells.

In the runs of our program, the maximum absolute value of the residuals after convergence in a time step was typically smaller than or about 10^{-7} . We used a time step $\Delta t = 2 \times 10^{-3}$ s. Results computed with a smaller time step of $\Delta t = 5 \times 10^{-4}$ s showed no significant differences with those obtained with the higher time step for selected cases. Note that Rosa *et al.* [9] adopted a time step of 10^{-3} s and Grigoletto *et al.* [14] used 10^{-4} s.

APPLICATION AND DISCUSSION

We first compare predictions from the proposed model with experimental measurements of the liquid holdup and pressure gradients taken from the comprehensive work of Hernandez-Perez [23] on gas-liquid two-phase flow in pipes. We extracted data for horizontal slug flows in pipes 6 m in length with diameters $D = 38$ and 67 mm. Table 1 contains the superficial velocities for each data point or run. He used water and air for the liquid and gas phases, respectively ($\rho_l = 1000$ kg m⁻³, $\mu_l = 10^{-3}$ kg m⁻¹ s⁻¹, and $\mu_g = 1.8 \times 10^{-5}$ kg m⁻¹ s⁻¹). The temperature was 20 °C and the pipe discharged to the atmosphere. The holdup and pressure sensors were located toward the pipe exit.

In the simulations, the liquid is assumed incompressible so that its density is constant throughout the pipeline. The outlet pressure was set to 101.3 kPa. We did not impose the restriction of evolving the first slug unit cell entering the pipe as steady — of course, after its generation based on the steady slug flow model. To have several slug units inside the pipe at a given time and to diminish inlet and outlet effects, we conducted the simulations with a pipe length of 20 m — the exception is Run 6 in which

Run	Liquid holdup		
	Experiment [23]	Model	Correlation 1 [25]
1	0.686	0.803	0.567
2	0.912	0.892	0.824
3	0.850	0.746	0.620
4	0.669	0.648	0.496
5	0.805	0.762	0.620
6	0.699	0.567	0.380

TABLE 2. EXPERIMENTAL VERSUS PREDICTED VALUES OF LIQUID HOLDUP FOR THE RUNS IN TABLE 1.

case we used a pipe length of 45 m because of the large size of each slug unit. We use the results obtained after 60 s of simulated physical time to avoid initial, strongly transient effects. As shown in Fig. 3 below, steady state is effectively attained well before 60 s. We are first interested in the slug unit liquid holdup and the pressure gradient. The liquid holdup for the entire slug unit is determined as a length-weighted average of the film holdup and the slug body holdup (equal to one). The pressure gradient is estimated by the difference between the pressures from corresponding locations in two consecutive slug unit cells, divided by the axial distance separating them. The sets of values for the holdup and pressure gradient computed in this manner are then averaged for the entire pipeline, excluding the contributions from the entering and exiting slug units, yielding the values reported here in Tables 2 and 3.

In the comparison, we include predictions from the correlations by Garcia *et al.* [24–26], which were obtained by fitting a large experimental database. From these works, we choose the correlations developed for the slug flow pattern. A correlation for the liquid holdup is given in [25] and labeled here as Correlation 1. References [24, 26] provide formulas for estimating the pressure drop; these are denoted here as Correlations 2 and 3, respectively.

From the results in Table 2, we find that the proposed model predicts the experimental liquid holdup of [23] with an average of the absolute value of the relative errors (AAVRE) of 9.8%, which is satisfactory. This AAVRE is defined as in equation (15) of [24]. On the other hand, values from Correlation 1 result in a higher average error AAVRE of 24.7%. Since the correlations represent fittings of experimental data, we also compare our model directly with the correlation. The relative difference between predictions from our model with those from Correlation 1 turns out to be large, with an AAVRE of 28.8%. Overall, predictions from our model are in between the experimental values and those from the correlation for the holdup — closer to the for-

Run	Pressure gradient (kPa m ⁻¹)			
	Experiment [23]	Model	Correlation 2 [24]	Correlation 3 [26]
1	0.180	0.024	0.031	0.030
2	0.276	0.196	0.227	0.219
3	0.416	0.239	0.281	0.273
4	0.286	0.295	0.332	0.369
5	0.425	0.118	0.138	0.135
6	0.302	0.178	0.199	0.239

TABLE 3. EXPERIMENTAL VERSUS PREDICTED PRESSURE GRADIENTS FOR THE RUNS IN TABLE 1.

mer. Regarding the pressure gradients (Table 3), Correlation 2 (Correlation 3) predicts the experimental measurements with an AAVRE of 41.9% (42.8%), whilst our model results in a slightly larger average error of 45.8%. These are unsatisfactory. On the other hand, the AAVRE between our model and Correlation 2 (Correlation 3) is 14.5% (16.7%) which is fairly good.

To perhaps improve the predictive capabilities of the model, we may consider modifying the net momentum flux in Eq. (19) with the inclusion of a head loss factor such as that applied by [14]. This considers the effect of the recirculation zone in the slug body near its front associated with the sudden expansion experienced by the liquid moving from the film to the slug body (with respect to a moving frame). Similarly, we may affect the momentum flux in (20) with a factor that accounts for the fact that the liquid does not suffer a sudden contraction moving into the film region, as imposed by the uniform film thickness approximation, but a gradual one resulting from the smooth profile of the bubble nose.

Other ways to improve the model include testing alternative friction factor correlations for the wall shear stress, especially in the slug body, and for the interfacial shear stress. Also, considering aerated slug bodies may affect the pressure gradient. In addition, trying other means for estimating the slug body length of the incoming slug unit — for instance, by introducing the slug frequency — and the wake effect in the bubble nose translational velocity may be promising.

Local liquid holdup spatio-temporal history observed with the steady and unsteady approaches for the first entering slug unit is shown in Figures 2(a) and 2(b) for the conditions of Run 3 in Table 1. In both cases, the liquid holdup history shows that propagation of the slug flow pattern to the outlet, located at the 20 m mark from the inlet, is achieved in about 12 s. Overall, no significant differences are observed for the holdup evolution between the two approaches. This spatio-temporal evolution is

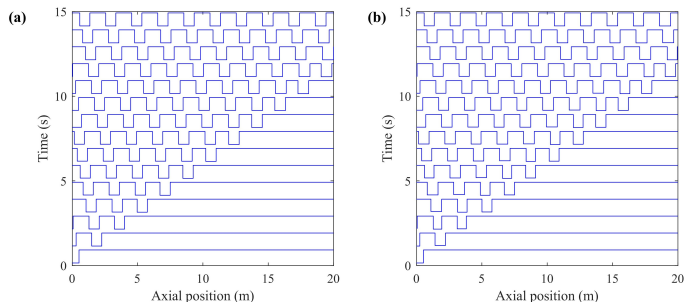


FIGURE 2. SPATIO-TEMPORAL EVOLUTION OF THE LOCAL LIQUID HOLDUP: (A) STEADY STATE APPROACH FOR THE FIRST SLUG UNIT; (B) UNSTEADY APPROACH. RESULTS ARE FOR RUN 3 OF TABLE 1.

closely related to the pattern observed in Fig. 3(a), where the pressure fluctuation associated with the first slug unit reaches the outlet at 12 s.

As shown in Fig. 3 (also for Run 3), near the start of the simulations, for $t = 0.1$ s (regardless of the treatment of the first slug unit), the pressure distribution in the fluid along the pipe axis has a constant gradient, spanning from about 110 kPa at the inlet to the atmospheric level at the outlet. During the first few seconds of the simulation, fluctuations of the pressure field develop very differently between the steady and unsteady approaches for the first slug unit. Figure 3(b) illustrates the occurrence of three pressure peaks with the maximum pressure at the inlet observed during the unsteady simulation: about 135 kPa at 0.5 s, 118 kPa at 2.8 s, and 110 kPa at 6.4 s. These relatively large peaks do not occur in Fig. 3(a). Pressure peaks in Fig. 3(b) are followed by the respective troughs, and the amplitude in general quickly decays.

The reason for the differences in the pressure behavior is related to the fact that, at the initial instant, there is a difference in the velocity of the fluid inside the pipe (liquid superficial velocity, j_l) and the velocity of the liquid in the incoming slug body just outside the pipe inlet (mixture velocity, $j_l + j_g$). This “jump” in the velocity is smoothed out for $t > 0$. With the steady approach for the first entering slug unit, the effect of this velocity difference on the gas dynamics of the bubble is significantly damped in comparison to the unsteady approach.

Beyond the 15 s of the simulation shown in Fig. 3, the pressure fluctuations in the unsteady simulation demonstrate average values and fluctuation amplitudes similar to the steady approach at all spatial instances. After 15 s, the inlet and outlet pressures oscillate around 105.75 kPa and 101 kPa respectively for both cases. Oscillation amplitudes for the steady approach are about 150 Pa and 350 Pa for the inlet and outlet pressure respectively, and about 300-350 Pa for both inlet and outlet pressure for the unsteady approach. The time history of pressure fluctuations in

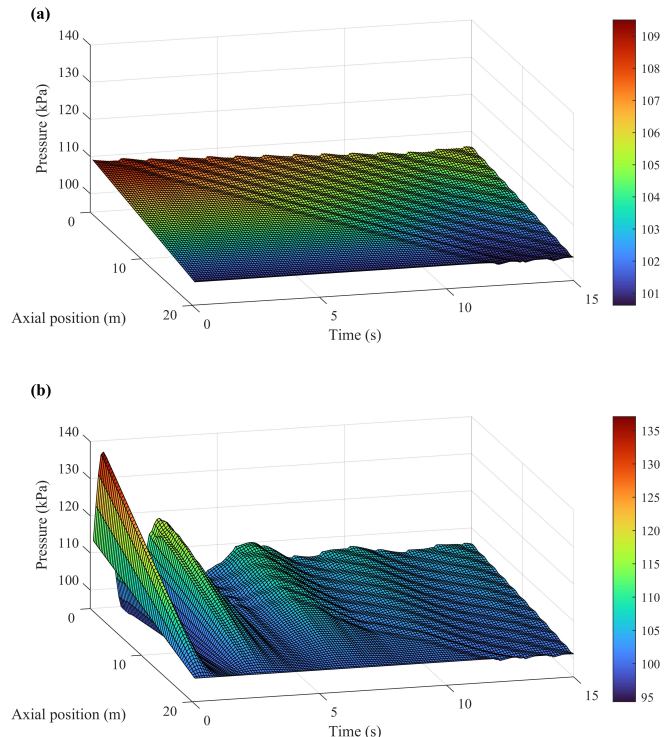


FIGURE 3. SPATIO-TEMPORAL EVOLUTION OF THE PRESSURE DISTRIBUTION: (A) STEADY STATE APPROACH FOR THE FIRST SLUG UNIT; (B) UNSTEADY APPROACH. RESULTS ARE FOR RUN 3 OF TABLE 1.

the unsteady case appears to be more complex for both inlet and outlet.

It would be useful in future work to obtain information from tracking selected slug units from the time they are inserted to the time they leave the pipe. Comparing the attributes of the first slug unit with those of a slug unit entering the pipe after that one has left may be revealing.

CONCLUDING REMARKS

In this work, we proposed a mechanistic model for unsteady gas-liquid slug flow in horizontal or inclined pipes (upward flow) with the slug tracking approach. The model is based on the mass and momentum conservation principles applied not only to the control volumes comprised within a typical slug-flow unit but also to the surfaces modeling the slug fronts and tails. At these locations, momentum balances result in jump laws for the pressure. Moreover, mass balances for transient conditions lead to non-uniform axial fluid velocity distributions for the liquid film and elongated bubble regions even in the case of a uniform film thickness.

Comparing with experimental data for horizontal slug flow,

model predictions of the slug unit liquid holdup are fairly good, contrasting with predictions of the pressure gradient, which yielded significant discrepancies, similar to those obtained from two correlations fitting a large experimental database. Comparing the model with the empirical correlations resulted in large differences for the liquid holdup; however, for the pressure gradient the performance of the proposed model is satisfactory.

There are several ways that the model's predictive capabilities could be improved or modified. One way includes modifying the momentum fluxes with factors that consider the actual configuration of the slug body front and tail regions. Another option is to apply alternative correlations in the model, for instance, for the friction factors, both for the wall and interfacial shear stresses.

In future work, we may include in the model the effects of a swarm of small gas bubbles traveling within the slug body. We also intend to model the random insertion process of slug units employing a random distribution of the slug body length as well as the associated process of merging of consecutive slug units.

ACKNOWLEDGMENT

This research is funded by the Engineering and Physical Sciences Research Council (EPSRC) of the UK Research and Innovation through the "MULTIPHASE FLOW-INDUCED FLUID-FLEXIBLE STRUCTURE INTERACTION IN SUBSEA APPLICATIONS (MUFFINS)" project grants EP/P033148/1 and EP/P033180/1.

NOMENCLATURE

A	Pipe cross sectional area.
$AAVRE$	Average of the absolute value of the relative errors.
$\bar{\alpha}$	Liquid holdup or void fraction in the elongated bubble-film region.
D	Pipe diameter.
g	Acceleration of gravity.
h	Thickness.
j	Superficial velocity.
l	Length.
μ	Phase viscosity.
N_u	Slug unit entering the pipe.
P	Pressure.
ρ	Phase density.
S	Perimeter.
σ	Interfacial tension.
t	Time.
τ	Shear stress.
u	Local phase velocity.
\bar{u}	Average phase velocity.
x	Slug body front position.
\dot{x}	Slug body front velocity.
y	Elongated bubble nose position.
\dot{y}	Bubble nose translational velocity.

z	Axial coordinate within the elongated bubble-film region'.
θ	Pipe axis inclination angle with respect to the vertical.
ζ	Spatial coordinate at a cross section.

Subscripts

e	Elongated bubble-film region tail.
f	Liquid film.
g	Gas.
l	Liquid.
o	Elongated bubble nose.
s	Slug body.
sx	Inside the slug body, at position x .
sy	Inside the slug body, at position y .
u	Unit cell.

Superscripts

j	Unit cell index.
m	Iteration index.
n	Time level.

REFERENCES

- [1] Dukler, A., and Hubbard, M., 1975. "A Model for Gas-Liquid Slug Flow in Horizontal and Near Horizontal Tubes". *Industrial & Engineering Chemistry Fundamentals*, **14**(4), pp. 337–347.
- [2] Taitel, Y., and Barnea, D., 1990. "Two-Phase Slug Flow". *Advances in Heat Transfer*, **20**(1), pp. 83–132.
- [3] Zhang, H.-Q., Jayawardena, S., Redus, C., and Brill, J., 2000. "Slug Dynamics in Gas-Liquid Pipe Flow". *Journal of Energy Resources Technology*, **122**(1), pp. 14–21.
- [4] Zhang, H.-Q., Wang, Q., Sarica, C., and Brill, J., 2003. "Unified Model for Gas-Liquid Pipe Flow via Slug Dynamics—Part 1: Model Development". *Journal of Energy Resources Technology*, **125**(4), pp. 266–273.
- [5] Shoham, O., 2006. *Mechanistic Modeling of Gas-Liquid Two-Phase Flow in Pipes*. Society of Petroleum Engineers, Richardson, TX.
- [6] Mazza, R., Rosa, E., and Yoshizawa, C., 2010. "Analyses of Liquid Film Models Applied to Horizontal and Near Horizontal Gas-Liquid Slug Flows". *Chemical Engineering Science*, **65**(12), pp. 3876–3892.
- [7] Issa, R., and Kempf, M., 2003. "Simulation of Slug Flow in Horizontal and Nearly Horizontal Pipes with the Two-Fluid Model". *International Journal of Multiphase Flow*, **29**(1), pp. 69–95.
- [8] Bonizzi, M., Andreussi, P., and Banerjee, S., 2009. "Flow Regime Independent, High Resolution Multi-Field Modelling of Near-Horizontal Gas-Liquid Flows in Pipelines". *International Journal of Multiphase Flow*, **35**(1), pp. 34–46.
- [9] Rosa, E., Mazza, R., Morales, R., Rodrigues, H., and Cozin, C., 2015. "Analysis of Slug Tracking Model for Gas-Liquid Flows in a Pipe". *Journal of the Brazilian Society*

- of *Mechanical Sciences and Engineering*, **37**(6), pp. 1665–1686.
- [10] Nydal, O., 2012. “Dynamic Models in Multiphase Flow”. *Energy & Fuels*, **26**(7), pp. 4117–4123.
- [11] Nydal, O., and Banerjee, S., 1996. “Dynamic Slug Tracking Simulations for Gas-Liquid Flow in Pipelines”. *Chemical Engineering Communications*, **141**(1), pp. 13–39.
- [12] Al-safran, E., Taitel, Y., and Brill, J., 2004. “Prediction of Slug Length Distribution Along a Hilly Terrain Pipeline Using Slug Tracking Model”. *Journal of Energy Resources Technology*, **126**(1), pp. 54–62.
- [13] Ujang, P., Lawrence, C., and Hewitt, G., 2006. “Conservative Incompressible Slug Tracking Model for Gas-Liquid Flow in a Pipe”. *BHR Group Multiphase Technology*, **5**, pp. 375–388.
- [14] Grigoletto, M. M., Bassani, C. L., Conte, M. G., Cozin, C., Barbuto, F. A., and Morales, R. E., 2021. “Heat Transfer Modeling of Non-Boiling Gas-Liquid Slug Flow using a Slug Tracking Approach”. *International Journal of Heat and Mass Transfer*, **165**, p. 120664.
- [15] Taitel, Y., and Barnea, D., 1990. “A Consistent Approach for Calculating Pressure Drop in Inclined Slug Flow”. *Chemical Engineering Science*, **45**(5), pp. 1199–1206.
- [16] Panton, R., 2013. *Incompressible Flow*, 4th ed. John Wiley & Sons.
- [17] Taitel, Y., and Dukler, A., 1976. “A Model for Predicting Flow Regime Transitions in Horizontal and Near Horizontal Gas-Liquid Flow”. *AIChE Journal*, **22**(1), pp. 47–55.
- [18] Cohen, L. S., and Hanratty, T. J., 1968. “Effect of Waves at a Gas-Liquid Interface on a Turbulent Air Flow”. *Journal of Fluid Mechanics*, **31**(3), pp. 467–479.
- [19] Talvy, C., Shemer, L., and Barnea, D., 2000. “On the Interaction Between Two Consecutive Elongated Bubbles in a Vertical Pipe”. *International Journal of Multiphase Flow*, **26**(12), pp. 1905–1923.
- [20] Katsikadelis, J. T., 2016. *The Boundary Element Method for Engineers and Scientists: Theory and Applications*. Academic Press.
- [21] Moin, P., 2010. *Fundamentals of Engineering Numerical Analysis*. Cambridge University Press.
- [22] Krasnopolsky, B. I., and Lukyanov, A. A., 2018. “A Conservative Fully Implicit Algorithm for Predicting Slug Flows”. *Journal of Computational Physics*, **355**, pp. 597–619.
- [23] Hernandez-Perez, V., 2007. “Gas-Liquid Two-Phase Flow in Inclined Pipes”. PhD Thesis, University of Nottingham, Nottingham, United Kingdom, September. See also URL <http://eprints.nottingham.ac.uk/11764/> (visited 28 April 2021).
- [24] Garcia, F., Garcia, R., Padrino, J., Mata, C., Trallero, J., and Joseph, D., 2003. “Power Law and Composite Power Law Friction Factor Correlations for Laminar and Turbulent Gas-Liquid Flow in Horizontal Pipelines”. *International Journal of Multiphase Flow*, **29**(10), pp. 1605–1624.
- [25] Garcia, F., García, R., and Joseph, D., 2005. “Composite Power Law Holdup Correlations in Horizontal Pipes”. *International Journal of Multiphase Flow*, **31**(12), pp. 1276–1303.
- [26] García, F., García, J., García, R., and Joseph, D., 2007. “Friction Factor Improved Correlations for Laminar and Turbulent Gas-Liquid Flow in Horizontal Pipelines”. *International Journal of Multiphase Flow*, **33**(12), pp. 1320–1336.